AIAA 94-0492

THE DEVELOPMENT OF A TUNABLE, SINGLE-FREQUENCY ULTRAVIOLET LASER SOURCE FOR UV FILTERED RAYLEIGH SCATTERING

N. Finkelstein, J. Gambogi, W.R. Lempert, and R.B. Miles
PRINCETON UNIVERSITY
Dept. of Mechanical & Aerospace Engineering
Princeton, New Jersey 08544 08544 U.S.A.

and

G.A. Rines, A. Finch, and R.A. Schwarz
SCHWARTZ ELECTRO-OPTICS, INC.
Concord, Massachusetts 01742 U.S.A.

32nd Aerospace Sciences Meeting & Exhibit
January 10-13, 1994 / Reno, NV

THE DEVELOPMENT OF A TUNABLE, SINGLE-FREQUENCY ULTRAVIOLET LASER SOURCE FOR UV FILTERED RAYLEIGH SCATTERING

N. Finkelstein, J. Gambogi, W.R. Lempert,* and R.B. Miles**

Dept. of Mechanical & Aerospace Engineering
PRINCETON UNIVERSITY
Princeton, New Jersey 08544 U.S.A.
609/258-2875

and

G. A. Rines, A. Finch, and R. A. Schwarz

SCHWARTZ ELECTRO-OPTICS, INC.
Concord, Massachusetts 01742 U.S.A.

ABSTRACT

We present the development of a flexible, high power, narrow line width, tunable ultraviolet source for diagnostic application. By frequency tripling the output of a pulsed titanium-sapphire laser, we achieve broadly tunable (227-360 nm) ultraviolet light with high quality spatial and spectral resolution. We also present the characterization of a mercury vapor cell which provides a narrow band, sharp edge absorption filter at 253.7 nm. These two components form the basis for the extension of the Filtered Rayleigh Scattering technique into the ultraviolet. The UV-FRS system is comprised of four pieces: a single frequency, cw tunable Ti:Sapphire seeding source; a high-powered pulsed Ti:Sapphire oscillator; a third harmonic generation system; and an atomic mercury vapor filter. In this paper we discuss the development and characterization of each of these elements.

1. INTRODUCTION

In recent years there has been significant activity in the development of optical diagnostic techniques which utilize high power laser systems coupled with narrow band vapor filters.[1-5] Most of this work has been directed to high speed flow field application, although, Shimizu et. al. have reported a vapor filter LIDAR approach for determining temperature in the mesopause.[6] To our knowledge, all of this work has utilized visible laser sources, such as second harmonic of Nd:YAG, Argon ion, or visible dye. While these systems have demonstrated significant potential, there are several distinct advantages of shifting into the ultraviolet: ultraviolet sources offer the advantage of both the frequency, ω^4, and the index-of-refraction, $(n-1)^2$, enhancement of Rayleigh and Raman scattering cross sections, and elastic 'flare' scattering from stray surfaces is reduced due to reduced reflectivity.[7] These features combine to produce greatly enhanced signal strength and image contrast in the ultraviolet. Finally, as will be shown, atomic mercury vapor filters exhibit nearly ideal characteristics.

The potential of UV-FRS is critically dependent upon the ability to produce a reliable, tunable, high-power, narrow linewidth, ultraviolet light source. The optical system we are developing, as illustrated in Fig. 1, is comprised of three principal components: a cw single-frequency, tunable Ti:Sapphire source, a pulsed Ti:Sapphire oscillator, which is injection-locked to the cw source, and a frequency tripler. A commercial Schwartz Electro-Optics Titan cw laser is modified to allow for continuous tuning in the near infrared. The cw source is used to injection-seed a high-power, pulsed, Ti:Sapphire laser, the output of which is passed through a set of third harmonic generating crystals. The result is a high-power, pulsed, near transform limited spectrally, near diffraction limited spatially, tunable ultraviolet laser source.

This source and the narrow-band, atomic-mercury vapor absorption filter constitute the key elements of a UV-FRS diagnostic measurement. In the following, we give a description of our progress to-date in the development of each component of the UV-FRS system. In particular, we present a detailed characterization of the

*Research Scientist, Mechanical & Aerospace Engineering, Member AIAA
**Professor, Mechanical & Aerospace Engineering, Senior Member AIAA

mercury absorption band at 253.7 nm, including both experimental absorption scans and spectral modeling.

2. DEVELOPMENT OF TUNABLE cw SOURCE

The goal of the cw source development effort is to generate continuously tunable, single frequency, near infrared laser light. Because the gain bandwidth of the titanium-sapphire is quite broad (680-1100 nm), it is an excellent medium for tunable laser sources. The laser is required to operate in both a high-power (1-3 Watt) and a low-power (milliwatt) regime for its two different tasks: cw mercury vapor spectroscopy, and high-power, pulsed oscillator seed source, respectively. Both tasks will be described in following sections.

By addressing the more taxing of the aforementioned goals, the multi-Watt level tunable output, we have been assured its success in operation as a spectroscopic tool and application as a seeder for the pulsed system. Figure 2 shows the schematic of the cw system. The Titan cw Ti:Sapphire laser system was pumped by a Coherent Inova 200 full-frame argon ion laser. Operated open cavity, the Ti:Sapphire laser system achieved 2.8 Watts of multi-mode output with 10 Watts of pump input. The cavity modes are spaced 250 MHz apart and the spatial mode is TEM_{00}.

To achieve single frequency, continuous scanning, the laser is operated in the ring configuration with a galvanometer-driven dual tilt plate assembly, and a piezo-electrically controlled scanning etalon. The coarse tuning element, a three-plate, bi-refringent filter, allows the laser to operate on one or more modes over a 15 GHz range. The tilt plates perform the continuous tuning by changing the effective cavity length.

The addition of a piezo-electric translator (pzt) driven etalon allows for single mode operation. The confocal air spaced etalon (Spectra Physics 761) is low finesse (approximately two, mirror reflectivity of 20%), and has a free spectral range of 75 GHz. By suppressing all other cavity modes below lasing threshold, the etalon acts to select the single, highest gain, longitudinal mode of the cavity. The single mode output is stabilized by adding a 2 kHz 'dither' to the etalon offset voltage, and by using a standard first derivative nulling[8] to provide feedback in the form of a quasi-dc bias voltage. The amplitude of the applied dither was 1 Volt, corresponding to a 100 MHz frequency modulation of the etalon, which produced a one milliwatt amplitude modulation of the laser power.

Calibration and linearity of the laser scan are essential for accurate spectroscopic characterization of the mercury vapor absorption. For this work, we have used a 1.5 GHz Fabry-Perot interferometer with custom built comparator circuit to monitor spectral continuity and linearity. A normal saw tooth ramp voltage was applied to the etalon at a much faster rate than the tuning of the laser. The comparator electronics consist of an analog sample and hold, which is triggered by the occurrence of an etalon transmission peak. The voltage applied to the etalon, which is proportional to the relative frequency change, was measured each time an etalon transmission occurred. Each point of the recorded offset voltages varied from a linear fit by less than 2 percent. Thus, we could verify a constant scan rate. The etalon traces also reveal any discontinuities, mode hops, or multi-mode behavior of the laser. The absolute frequency of the system is determined by calibration with low pressure mercury vapor absorption, which will be discussed in detail below.

This single etalon and tilt-plate combination was found to reliably produce single-frequency tunable output. The laser system achieved 2.2 Watts single longitudinal mode tunable output at 761 nm, with 10 Watts of ion laser pump power. It could be reliably tuned, continuously, in excess of 15 GHz without adjustment of the bi-refringent filter. With appropriate tuning of the bi-refingent filter (micro-motor attachment and control), we anticipate that the system could be tuned for much greater (order of nanometer) intervals. The linearity of the tuning mechanism is better than 98% over 15 GHz, with the spectral line width approximately 1 MHz over milliseconds, and approximately 10 MHz over minutes.

3. DEVELOPMENT OF THE PULSED SYSTEM

The ultimate purpose of the scanning cw system is to act as a seeder for a high-power, pulsed, injection-locked system, that will be used for diagnostic techniques such as UV Filtered Rayleigh Scattering. It is relatively straightforward to injection seed a high-power oscillator. However, without active feedback to adjust the pulsed laser cavity length, the output frequency will fluctuate between one and two longitudinal mode output.[9] When the seed laser frequency closely matches the resonance condition of the pulsed oscillator, the output is single mode. When the frequency of the seed beam lies between two cavity modes of the pulsed oscillator, the laser operates on both cavity modes. In the single mode case, the output is a near the transform-limited spectral line width; whereas, in the dual mode case, the output is 2.5 to 3 times the transform-limit, spectrally. For UV-FRS it is desirable to continuously scan, while maintaining true single mode frequency output. To this end, we are in the process of developing a control system to acquire and maintain single longitudinal mode operation.

The schematic of the injection seeded Ti:Sapphire system is given in Fig. 3. The second harmonic output (at 532 nm.) of a Continuum model YG-661 Nd:YAG laser serves as the pump for a breadboard version of a Schwartz Electro-Optics pulsed Ti-Sapphire laser. It is significant to note that the spatial mode of the Nd:YAG pump is near TEM_{00}. This requires the Ti:Sapphire crystal to be located at the intermediate field of the two focusing lenses, F1 and F2, in order to prevent surface

damage. After some experimentation, nominal 130 cm focal length lenses were positioned 70 cm in front of the Ti:Sapphire crystal faces. The cavity is purposely seeded in a lossy fashion. This provides a simple means of optical isolation of the cw cavity from high-power, pulsed light feedback. The cw seed signal is coupled into the pulsed oscillator cavity using the first turning prism, which is designed to be slightly off Brewster's angle, resulting in approximately 0.5% reflectivity. As needed, other optical isolators, lossy mirrors or Faraday isolators, are added. Approximately 100 microwatts is sufficient for seeding.

Some preliminary work has been done to demonstrate locking of the pulsed laser to the seed (cw) laser. The control system takes advantage of the fact that the pulsed resonator design is inherently low-Q, and, therefore, acts as an external cavity Fabry-Perot etalon for the cw seeding beam. Tuning the cavity length produces Fabry-Perot fringes with a modulation depth of approximately 50%, which can be easily detected by placing a photodiode detector behind the high reflector. Cavity stabilization was demonstrated by locking to a 'side' of the fringe at approximately the half height of the fringe. The locking was performed with a simple comparator circuit which returned a voltage proportional to the difference between the actual fringe transmission, and a variable reference value. The feedback signal is applied to the piezo-electrically mounted output coupler. Single frequency, pulsed operation, as determined by observation of a smooth temporal pulse profile, was achieved in the laboratory for periods on the order of minutes, although the seed laser could not be significantly tuned because of the rudimentary locking electronics.

For our purposes, there are distinct advantages of the fringe-locking mechanism over the standard pulse build-up minimization technique. The main difference between these two control systems is that the fringe, cavity resonance system offers continuous feedback, while the pulse build-up minimization system offers only shot-to-shot feedback. This latter mechanism of feedback control is most accurate when the pulse conditions are not rapidly changing. As a result, scanning must be very slow. Further, the effects of unstable ambient noise are not accounted for. By continuously monitoring the seed beam (except during the actual firing of a pulse), the fringe monitoring control allows for greater stabilization in less stable environments.

We are currently in the process of implementing a higher bandwidth, more robust version of the fringe-locking approach, based on the ramping of the piezo-electric material bias voltage through several fringe orders prior to each firing of the pulsed laser. A similar approach has been developed by workers at NIST in an injection-seeded, flashlamp-pumped ring dye laser.[10] It is anticipated that this system will provide continuous tuning capability, and control bandwidth on the order of 100 kHz.

The resulting system yields high energy, single longitudinal mode output over a widely tunable range in the near infrared. The system produces 100 mJ/ pulse output in a 7 nsec pulse at 10 Hz, pumped at 280 mJ/ pulse at 532 nm. The spatial quality is TEM_{00} and nearly diffraction limited.

4. THIRD HARMONIC GENERATION

Third harmonic generation is performed in the standard two step manner: type I doubling of the fundamental, and subsequent type II mixing of the residual fundamental with the second harmonic produced in the first step. Beta Barium Borate (BBO) is used for both steps. Figure 4 shows the conversion to third harmonic as a function of fundamental energy per pulse. The advantages of seeded operation are clearly evident. Seeding improves the spatial mode quality and reduces the bandwidth, both of which enhance the harmonic generation. Second harmonic generation is near the optimum of 67% internal conversion by power, or 50% conversion by photon. The conversion from the second to third harmonic is considerably lower, and results in a net conversion to third harmonic of 14% to 18%.

The same scheme is used for generation of cw tunable ultraviolet light; however, due to much lower power, a pair of BBO crystals is used in a wedged walk-off compensating geometry to produce the second harmonic. The dual crystal arrangement increases the second harmonic conversion by creating a longer effective interaction length than can be generated with a single crystal (due to walk-off of the Poynting and propagation vectors). The generation of third harmonic is identical to the pulsed set-up. Because of the low power, only trace amounts of tunable ultraviolet light is created (on the order of 10^{-10} Watts). However, as we will demonstrate in the following section, this is sufficient to perform the Hg vapor spectroscopy.

5. CHARACTERIZATION OF THE MERCURY FILTER

Accurate characterization of the absorption spectra of optically thick mercury vapor is essential if it to be used as a filter medium. Appropriate characterization is critical for diagnostics which depend upon the knowledge of the filter profile to measure flow properties such as temperature, velocity, and density. Additionally, predictive modeling capability allows for construction of filters most appropriate to given experimental conditions. Characterization of the mercury filter is achieved by measuring transmission as a function of laser frequency. Computer models are used to quantify appropriate parameters such as maximum attenuation, and homogenous versus inhomogeneous broadening ratios.

Ideally, an atomic or molecular vapor filter will completely suppress background scattering while transmitting all Rayleigh or Raman scattered light. Four salient features characterize an ideal filter: infinitely sloped edges (to allow for a precise filter frequency cut-off), zero transmission over the entire width of the absorption band, unity transmission outside the filtering band, and a variable width filtering band.

Our mercury filter, consisting of a 5 cm. long by 5 cm. diameter all quartz cell with an 18 cm. side arm 'cold' tip, is shown in Fig. 5. The cell body, excluding the side arm portion, is wrapped in heating tape which controls the body temperature to ± 1 C. A water bath encloses the side arm and maintains constant temperature to ± 0.1 C. Prior to sealing, a small quantity (approximately 5 gms) of electronic grade mercury was inserted and the cell evacuated. The pressure inside the cell is estimated to be less than 0.05 torr. Since the heating tape maintains the cell body at a temperature higher than that of the water bath, the side arm temperature controls the vapor pressure of the mercury. Experiments were run characterizing the mercury absorption at side arm temperatures of 23 C, 70 C, and with the water bath replaced by a CO_2 slurry. These corresponds to vapor pressures of 0.0015 torr, 0.048 torr, and less than 10^{-5} torr, respectively.

The experimental set-up for the absorption experiments is depicted in Fig. 2. The tunable output of the cw Ti:Sapphire laser is frequency-tripled, as previously described. A prism separates the fundamental and second harmonic from the 253.7 nm which is 50:50 split into reference and absorption legs. Twenty nanometer bandwidth interference filters are used in combination with solar blind photomultiplier tubes to avoid interference from scattered second harmonic light. The signal from the photomultiplier tubes is filtered through a low band-pass RC circuit (time constant of 0.01 seconds), and digitized with a laboratory computer based A/D system. The computer also collects a signal from the custom built comparator circuit which measures the relative frequency axis, as described previously. Complete (100%) transmission is determined by removing the cell from the beam path.

Figure 6 is a transmission profile of the mercury cell with a side-arm temperature of 23 C, and a body temperature of 48 C. This scan represents a sweep of approximately 30 GHz in the UV, or 10 GHz in the fundamental. Five strong, and one weak absorption lines are clearly evident. These different lines arise from the six different naturally-occurring isotopes of mercury. The isotopes are listed above their corresponding absorption lines. The odd isotopes have non-zero nuclear spin which produces hyperfine splitting. The even isotopes have zero nuclear spin and therefore each produces a single transition. The relative frequencies of these absorption bands agree well with earlier published values, which are represented as vertical lines on the bottom of the figure.[11] The square-bottomed shape of the five strong absorption lines is characteristic of optically thick absorption (i.e. the absorption coefficient multiplied by the cell length is much greater than one). The Hg 196 absorption profile is not optically thick because of its low natural abundance of 0.14%. Between the discrete absorption bands we see an approximately flat transmission, at about 70% of the signal without the cell present. The 30% loss is due to the four uncoated window surfaces of the cell. With the beam blocked, a slight offset from zero exists corresponding to 1 nA of photomultiplier tube dark current.

A blow-up of the Hg 202 isotope absorption feature is given in Fig. 7, along with a computer model assuming a Voigt spectral lineshape. The figure demonstrates mercury's nearly ideal characteristics as a vapor filter. The sharp edges and flat base are characteristic of this very optically thick case. The modeling corresponds to an optical depth of approximately 71. [Line center attenuation is exp(-71) or 10^{-31}]. The 10% to 90% absorption edge occurs over 0.55 GHz, while the full width half maximum is 2.76 GHz. In Fig. 7, the Lorentzian component (FWHM) is fixed at 2.66 MHz, based on the mercury excited state natural lifetime of 120 nanoseconds. The Gaussian component (FWHM) is 1.067 GHz, corresponding to the cell body temperature of 48 C.

The measurement at the dry ice cold tip temperature verified that the 70% baseline transmission is due to window losses as opposed to continuum background absorption, which limits the extinction Iodine vapor-based cells.[12] This high off-line transmissivity allows for greater flexibility in design of vapor filter absorption bands, since the absorption characteristics (extinction and bandwidth) may be widely varied by altering the 'cold' tip temperature.

As an example of this, the side-arm was heated to 70 C, which increases the vapor pressure to 0.05 torr, and the optical depth to approximately 2000 (or maximum attenuation of 10^{-850}). The cell temperature was kept at 105 C, which yields an inhomogeneous linewidth of 1.19 GHz (FWHM). As can be seen in Fig. 8, the width of the absorption band also increases rather dramatically. For naturally occurring isotopic abundance of mercury, the once separate absorption lines are no longer fully resolved. The fwhm of an individual absorption line increases from 2.76 Hz at 23 C, to an estimated 4.6 GHz at 70 C. Another significant feature, evident from Fig. 8, is the distinct presence of Lorentzian 'wings' on the absorption profile. Preliminary models verify the existence of this non-negligible Lorentzian wing assuming a linewidth of 2.66 MHz, or 0.22% of the 1.19 GHz Gaussian component. The Lorentzian contribution appears in the wings of the very optically thick Voigt profile, where it dominates due to its $1/\Delta\omega^2$ frequency profile off line center. The significance for diagnostic measurements is that this represents a fundamental limit to the filter cut-off under extreme optically thick conditions.

To summarize, in examining the three mercury absorption spectra, the following salient features have been observed. In the optically thick regime, absorption lines appear to have sharp edges and flat bases. In our reference case of a 23 C, 5 cm length cell, we model an optical depth of approximately 71, and spectral bandwidth (FWHM) of 2.76 Hz. The bandwidth and optical depth may be varied significantly by altering the cold tip temperature; however, under extreme optically thick conditions, the Lorentz component becomes significant in the near wings. No measurable continuum absorption or other absorption features were observed.

6. CONCLUSIONS

The key elements of a flexible, high-power, single-frequency tunable ultraviolet source for diagnostic applications such as UV FRS have been demonstrated. A cw tunable, single-mode Ti:Sapphire laser has been constructed for use as a seeder for a pulsed titanium sapphire system, and as an independent cw spectroscopic tool. Detailed characterization of a mercury vapor absorption filter has shown it to exhibit nearly ideal characteristics, including exceedingly high line center attenuation, flat bottoms and sharp edges, variable bandwidth, and freedom from spectral interference.

ACKNOWLEDGMENTS

The authors wish to acknowledge G. Scoles, K. Lehmann, and M. Souza for useful discussions, and P. Howard for providing technical assistance. This research was conducted with support from AFOSR, M.L. Energia, Inc., and NASA-Ames.

REFERENCES

1. R.B. Miles and W.R. Lempert, Appl. Phys B 51, p.1 (1990).

2. G.S. Elliott, M. Samimy, and S.A. Arnette, AIAA-92-0175 (1992).

3. H. Komine, S.J. Brosnan, A.B., Litton, and E.A. Stappaerts, AIAA-91-0337 (1992).

4. J.A. Shirley and M. Winter, AIAA-93-0513 (1993).

5. J.W. Lee, J.F. Meyers, A.A. Cavone, and K.E. Suzuki, AIAA-93-0414 (1993).

6. H.S. Shimizu, S.A. Lee, and C.Y. She, Appl. Opt. 22, p. 1373 (1983).

7. D.E. Gray, *American Institute of Physics Handbook*, 2nd ed., p. 6-119 (1963).

8. G.C. Bjorkland, Opt. Lett. 5, p. 15 (1980).

9. R.L. Schmidt and L.A. Rahn, Appl. Opt. 25, p.629 (1986).

10. G.J. Rosasco, W.J. Bowers, W.S. Hurst private communication. Nation Institute of Standards and Technology, Process Measurements Division, Gaithersburg, MD.

11. F. Bitter, Appl. Opt., 1, p. 1 (1962).

12. R.B. Miles, J.N. Forkey, and W.R. Lempert, AIAA-92-3894 (1992).

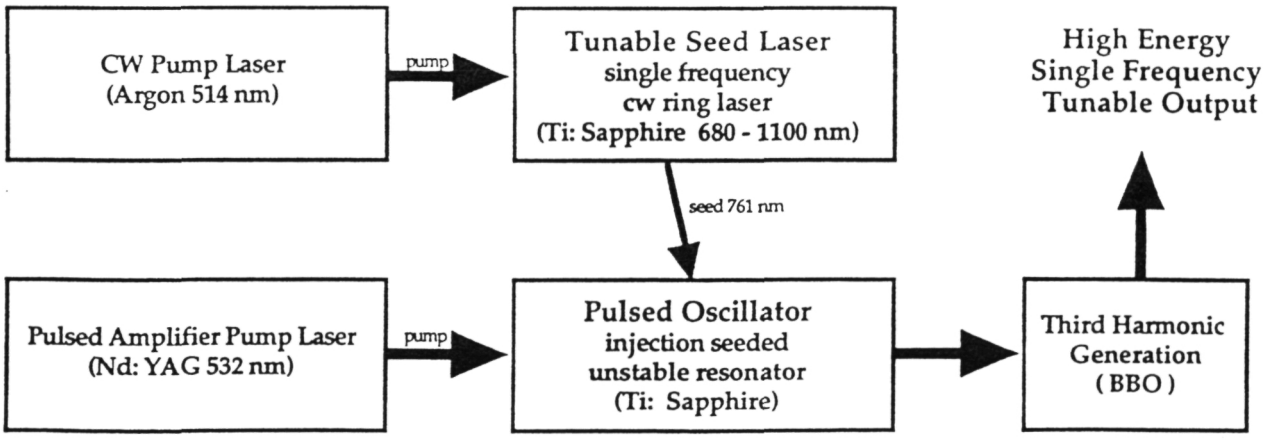

Fig. 1. Tunable single-frequency ultraviolet source.

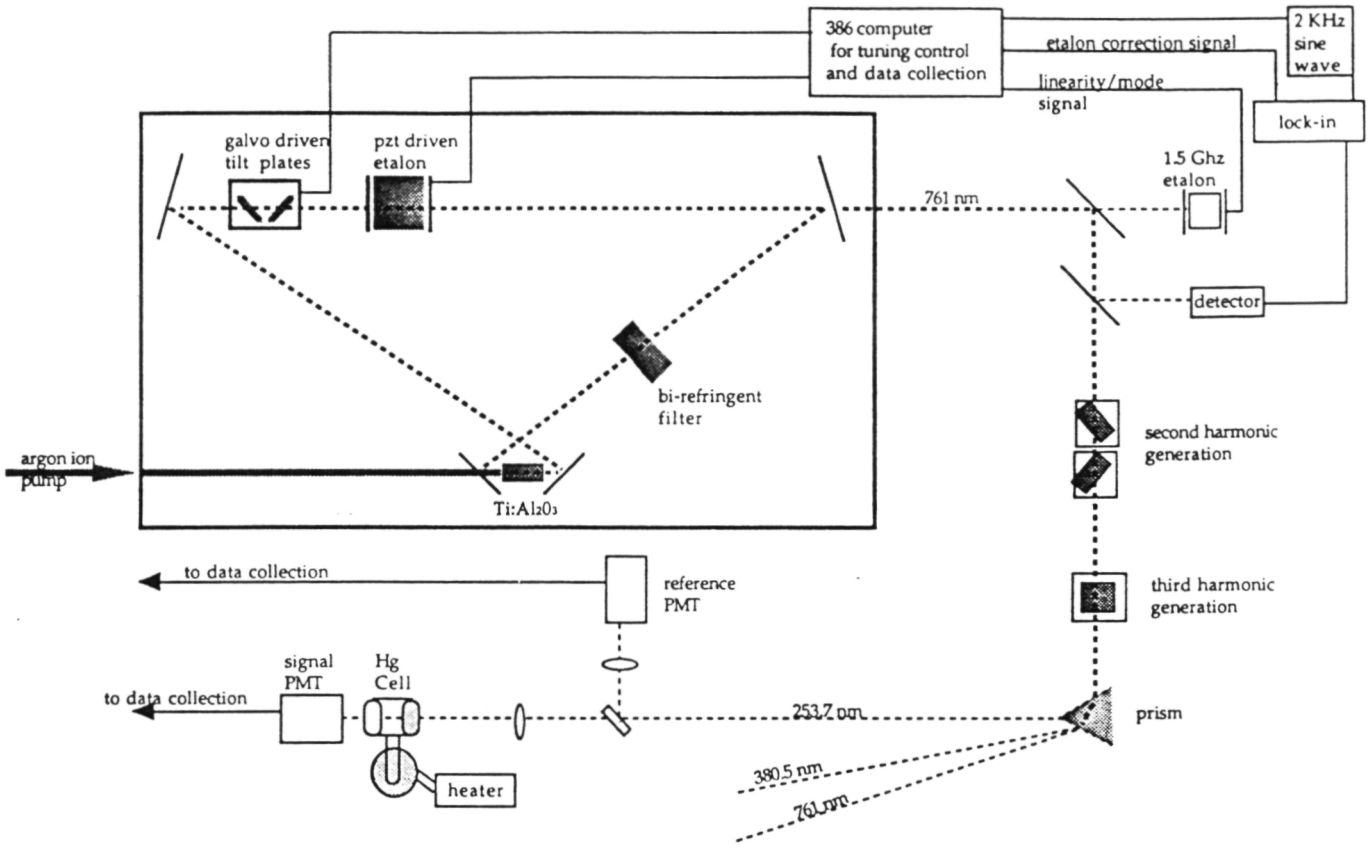

Fig. 2. cw Ti:Sapphire laser schematic with Hg spectroscopy experiment.

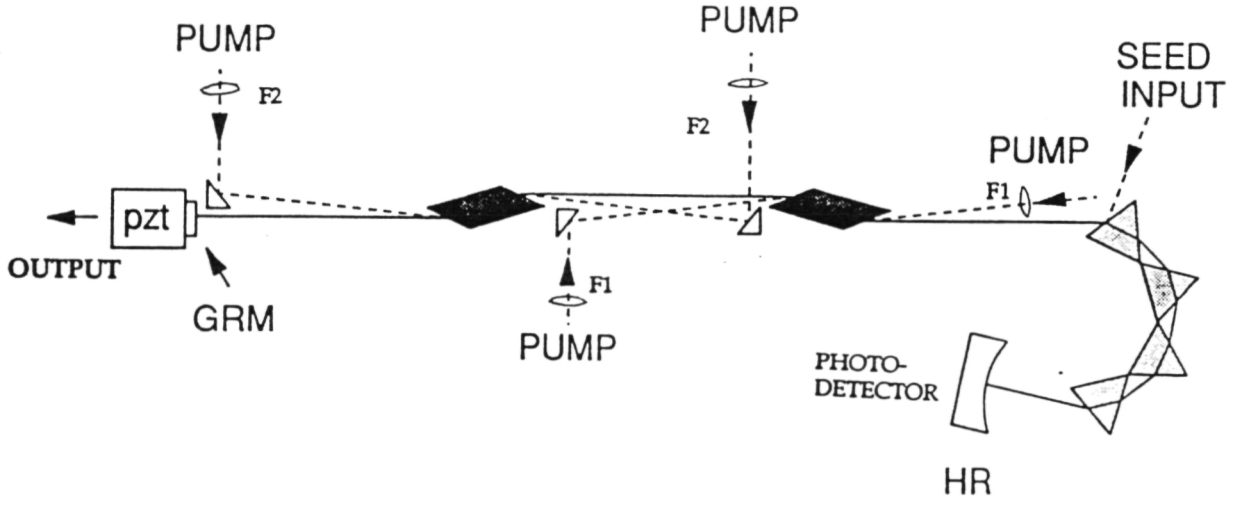

Fig. 3. Schematic illustration of pulsed laser oscillator.

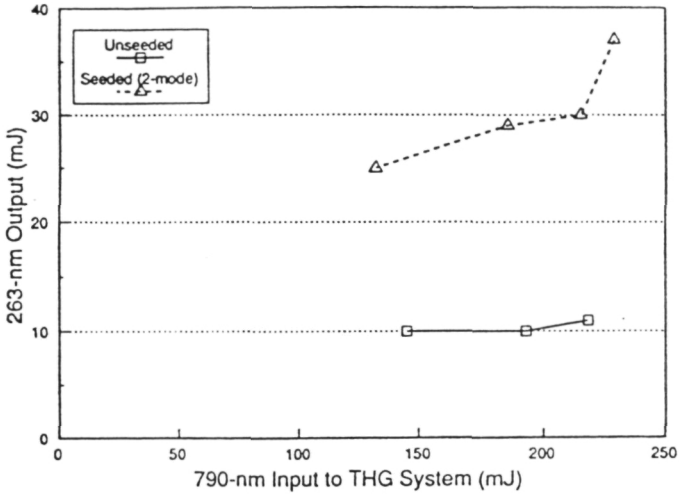

Fig. 4. Third-harmonic conversion efficiency at 790 nm.

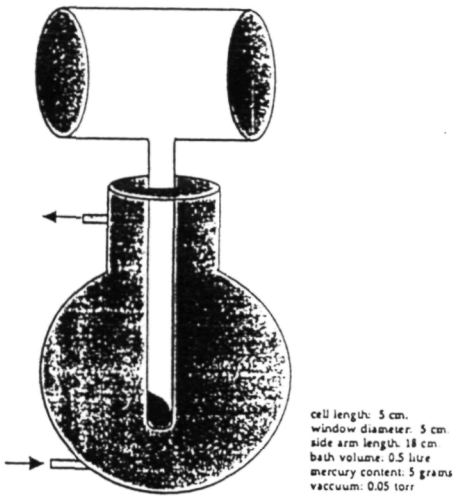

Fig. 5. Schematic illustration of mercury vapor cell and water bath.

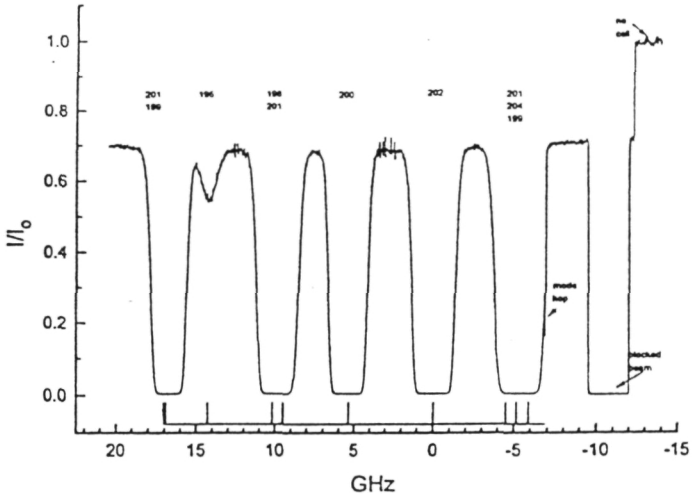

Fig. 6. Experimental Hg absorption with side-arm temperature of 23C, and cell body temperature of 48C.

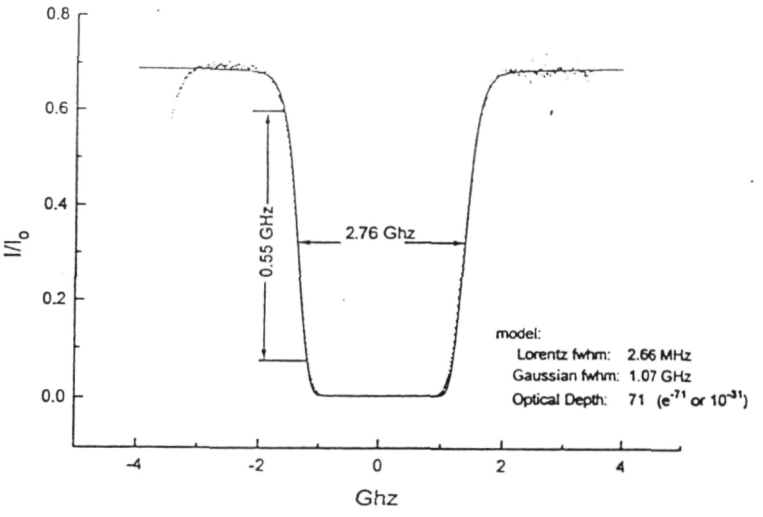

Fig. 7. Blow-up of experimental data (dotted) from Fig. 6 in vicinity of Hg 202 transition, along with modeling prediction (solid).

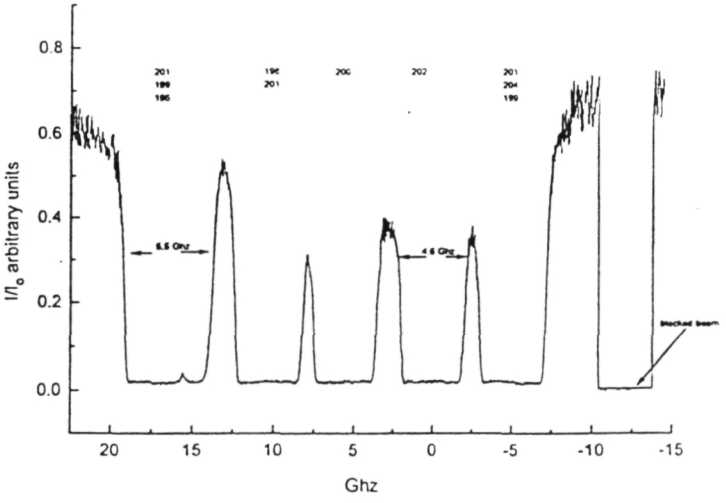

Fig. 8. Experimental Hg absorption with side-arm temperature of 70C, and cell body temperature of 105C.